Impairment-aware Virtual Network Embedding Using Time Domain Hybrid Modulation formats in Optical Networks

Materials and Design 194 (2020) 108915

Contents lists available at ScienceDirect

Materials and Design

journal homepage: www.elsevier.com/locate/matdes

# Surface potential and roughness controlled cell adhesion and collagen formation in electrospun PCL fibers for bone regeneration

Sara Metwally [a], Sara Ferraris [b], Silvia Spriano [b], Zuzanna J. Krysiak [a], Łukasz Kaniuk [a], Mateusz M. Marzec [c], Sung Kyun Kim [d], Piotr K. Szewczyk [a], Adam Gruszczyński [a], Magdalena Wytrwal-Sarna [c], Joanna E. Karbowniczek [a], Andrzej Bernasik [c,e], Sohini Kar-Narayan [d], Urszula Stachewicz [a,*]

[a] International Centre of Electron Microscopy for Materials Science, Faculty of Metals Engineering and Industrial Computer Science, AGH University of Science and Technology, Cracow, Poland
[b] Department of Applied Science and Technology, Politecnico di Torino, Turin, Italy
[c] Academic Centre for Materials and Nanotechnology, AGH University of Science and Technology, Cracow, Poland
[d] Department of Materials Science and Metallurgy, University of Cambridge, Cambridge, United Kingdom
[e] Faculty of Physics and Applied Computer Science, AGH University of Science and Technology, Cracow, Poland

## HIGHLIGHTS

- Applied voltage polarity in electrospinning tailors surface chemistry and potential of PCL fibers.
- Surface potential was analyzed by KPFM and compared with zeta potential in liquid.
- Cell adhesion, collagen formation and mineralization are controlled with surface potential.
- Surface potential on PCL fibers can enhance the bone regeneration process.

## GRAPHICAL ABSTRACT

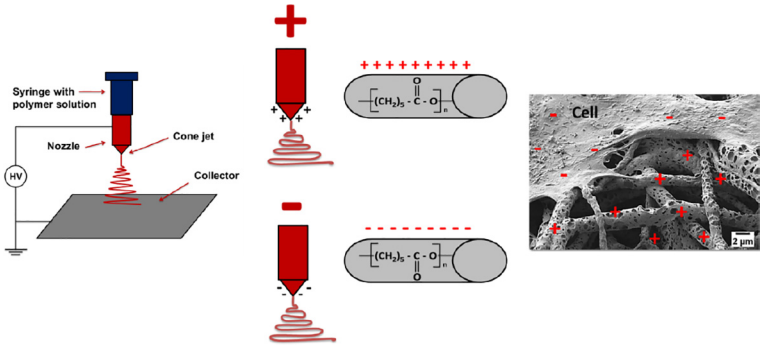


## ARTICLE INFO

*Article history:*
Received 28 April 2020
Received in revised form 18 June 2020
Accepted 21 June 2020
Available online 25 June 2020

*Keywords:*
Surface potential
Kelvin probe force microscopy
Zeta potential
Cells
Adhesion
Mineralization

## ABSTRACT

Surface potential of biomaterials is a key factor regulating cell responses, driving their adhesion and signaling in tissue regeneration. In this study we compared the surface and zeta potential of smooth and porous electrospun polycaprolactone (PCL) fibers, as well as PCL films, to evaluate their significance in bone regeneration. The ' surface potential of the fibers was controlled by applying positive and negative voltage polarities during the electrospinning. The surface properties of the different PCL fibers and films were measured using X-ray photoelectron spectroscopy (XPS) and Kelvin probe force microscopy (KPFM), and the zeta potential was measured using the electrokinetic technique. The effect of surface potential on the morphology of bone cells was examined using advanced microcopy, including 3D reconstruction based on a scanning electron microscope with a focused ion beam (FIB-SEM). Initial cell adhesion and collagen formation were studied using fluorescence microscopy and Sirius Red assay respectively, while calcium mineralization was confirmed with energy-dispersive x-ray (EDX) and Alzarin Red staining. These studies revealed that cell adhesion is driven by both the surface potential and morphology of PCL fibers. Furthermore, the ability to tune the surface potential of electrospun PCL scaffolds provides an essential electrostatic handle to enhance cell-material interaction and cellular activity, leading to controllable morphological changes.



* Corresponding author.
*E-mail address:* ustachew@agh.edu.pl (U. Stachewicz).

https://doi.org/10.1016/j.matdes.2020.108915

## 1. Introduction

Controlling the mineralization process is crucial for bone tissue engineering, as both hydroxyapatite (HAp) and collagen are key elements of the bone matrix. Each type of cell shows an individual and unique response to surface charge and potential, determining the adhesion, collagen mineralization, and tissue formation process [1]. Positively charged surfaces have been shown to significantly influence cell proliferation and spreading, activate the signaling cascade of the immune system, and accelerate the regenerative response [2,3]. Hence, understanding the effect of surface charge is key to designing biomaterials for specific tissue engineering applications. However, the current knowledge on surface charge and its potential impact on cell-material interaction is still rather limited.

The most common parameter describing the surface potential of biomaterials in contact with a liquid is the zeta potential ($\zeta$), which is the potential developed at the material-liquid interface, and its precise measurement is crucial for designing biomaterials interfaces. Note that surface charge depends on the environmental conditions. Upon contact with a liquid solution, functional groups of the material are protonated or ionized forming the electrical double layer (Stern- Graham and Gouy–Chapman diffuse layer), and the zeta potential is typically measured at the shear plane between the two layers [4]. The surface charge of the biomaterials is also described by the isoelectric point (IEP), defining the pH value where the zeta potential is zero [5]. IEP influences protein adsorption, which directly affects cell responses [6]. Proteins tend to adsorb more readily near their IEP, due to reduced electrostatic repulsion with other proteins on the materials' surface. Proteins determine the initial cellular and subsequent host responses [7]. At the same time, cell-biomaterial electrostatic interactions are critical in the first phase of cell adhesion [8]. Surface charge and potential determine the amount, type, and refolding degree of proteins adsorbed on the surface, which in turn influence the cell adhesion process, integrin bonding, and focal adhesion formation [9]. In the case of collagen, the zeta potential is affected by pH and it exhibits an IEP of 9.3. Importantly, it was found that the charged groups in collagen provide nucleation sites that induce nucleation of the apatite [10]. Other in vivo experiments demonstrated that osteoblasts concentrate calcium phosphate within intracellular compartments, which is then delivered to the collagen at the bone growth front, where it infiltrates the fibrils and crystallizes into apatite [11].

The surface charge of biomaterials, such as electrospun fibers, is most often tuned by surface chemical modifications [12]. However, in the present study, the surface potential of the fibers was controlled by applying positive and negative voltage polarity to the nozzle during the electrospinning process [13,14]. The changing polarity of the applied voltage enables control of the molecular orientation of the chemical functional groups in the polymers chains [15]. Electrospinning with negative polarity causes the accumulation of negative charges at the surface of the liquid jet, leading to the dipoles within the polymer to be orientated under the influence of the electric field [2,16]. By this process, we have been able to tailor the surface potential of electrospun fibers, and thus control the surface potential developed in contact with physiological liquids.

PCL is one of the most widely used polymers in tissue engineering [17], however, there is a lack of study on the effect of surface potential and charge of PCL, and the influence of these on cell adhesion and collagen mineralization. Therefore, in this study, we produced smooth and porous PCL fibers by applying positive and negative voltage polarity to the nozzle during electrospinning in order to investigate cell responses in relation to surface potential. Here, we clearly show the ability to control both the surface charge and morphology of PCL fiber scaffolds in a single-step process, without the need of surface chemical modifications, for controlled cell adhesion, filopodia formation, collagen and calcium mineralization. These processes are highly desirable in regenerative medicine, and we demonstrate here a way to achieve these using electrospun PCL fibers whose surface potential can be tuned by the voltage polarity used during the electrospinning process.

## 2. Materials and methods

### 2.1. Materials

The smooth PCL fibers were produced from 12% solution of poly (ε-caprolaptone) (PCL) (CAPA 6500, $M_w = 50{,}000\ g \cdot mol^{-1}$, Perstorp, UK) dissolved in chloroform, while the porous fibers were produced from 12% PCL solution dissolved in a mixture of chloroform and dimethylsulfoxide (DMSO) in the ratio 90:10 v/v.

### 2.2. Electrospinning and spin coating

We prepared three different types of scaffolds: (1) smooth PCL fibers, (2) porous PCL fibers, and (3) PCL films that were used as reference samples. PCL fibers were produced by applying either positive or negative voltage polarities to the nozzle during the electrospinning process, using the electrospinning apparatus EC–DIG (IME Technologies, the Netherlands). The smooth PCL fibers (1) were electrospun by applying a voltage of ±12 kV to the nozzle, while maintaining a solution flow rate of $0.5\ mL \cdot h^{-1}$ and a distance of 15 cm between the nozzle and the collector. The fibers were electrospun in a climate-control chamber at a temperature of 25 °C and a humidity of 50%. The porous PCL fibers (2) were electrospun by applying ±14 kV to the nozzle, while maintaining a solution flow rate of $1\ mL \cdot h^{-1}$ and a distance of 20 cm between the nozzle and the collector. The temperature was set at 25 °C, while the humidity was increased to 70%. The PCL film (3) was prepared from solution on a glass slide using a spin-coater (L2001A v.3, Ossila, UK). A volume of 0.1 mL was deposited on the glass slide and spun for 60 s with a rotation speed of 6000 rpm at a temperature of 22 °C and humidity of 30%. Note that for the PCL film, we used the same solution prepared for the smooth PCL fibers.,

### 2.3. Scanning electron microscopy (SEM) and surface profilometry

The scaffolds and cell-material interactions were studied with SEM (Merlin Gemini II, Zeiss, Germany). Prior to SEM imaging, samples were coated with a 5 nm gold layer using rotary-pumped sputter coating (Q150RS, Quorum Technologies, UK). All of the samples were imaged in the SEM by applying a current of 20 pA and voltage of 3 kV. Fiber diameters and pore sizes were measured from the SEM images using Fiji (Life-Line Version 2.0, USA).

To verify the average surface roughness ($R_a$), fibers were deposited on 16 × 16 mm glass slides. The surface profilometry was verified based on scanning up to 640 $\mu m^2$ area for all of the samples using Laser Microscopy (Olympus OLS4000, Japan).

### 2.4. Contact angle measurement

The advancing contact angle was measured on PCL fibers using deionized water (Spring 5UV purification system, Hydrolab, Poland), phosphate-buffered Saline (PBS), and Dulbeccos' Modified Eagle Medium (DMEM) (Sigma Aldrich, UK). The surface tension of all liquids have been reported previously [2]. Droplets with a volume of 3 μL were deposited onto surfaces and the images were taken using a Canon EOS 700D camera with EF-S 60 mm f/2.8 Macro USM zoom lens. The contact angles were measured using MB ruler 5.3 software.

### 2.5. X-ray photoelectron spectroscopy (XPS)

Prior to XPS analysis, PCL fibers and films were deposited onto 16 × 16 silicon wafers and coated with approximately 20 nm gold layer. The surface chemistry of PCL fibers and films were analyzed using angle-resolved XPS (PHI Versa Probe II Scanning XPS system, Ulvac-Phi,

Chigasaki, Japan) with monochromatic Al Kα (1486.6 eV) X-rays focused to a 100 μm spot. The photoelectron take-off angle was set to 15° to obtain information from the topmost layer of the material. The pass energy in the analyzer was set to 46.95 eV to obtain high energy resolution spectra for the C 1s and O 1s regions. A dual beam charge compensation with 7 eV Ar + ions and 1 eV electrons were used to maintain a constant sample surface potential regardless of the sample conductivity. All XPS spectra were charge referenced to the unfunctionalized, saturated carbon (C—C) C1s peak at 284.8 eV. The operating pressure in the analytical chamber was less than $4 \times 10^{-9}$ mbar. The deconvolution of the spectra was carried out using PHI MultiPak software (v.9.8.0.19). The spectrum background was subtracted using the Shirley method.

### 2.6. Kelvin probe force microscopy (KPFM)

KPFM was used to measure the surface electric potential of PCL samples in ambient conditions [18]. These atomic force microscopy (AFM) based measurements were performed using Bruker Multimode 8 (Bruker, USA). For all the measurements, conducting MESP-RC-V2 cobalt-chromium coated tips (Bruker, USA) with a nominal spring constant of 5 $Nm^{-1}$ were used. KPFM was performed on fibers having a similar diameter across all PCL samples to minimize the size effect on the measurements. Standard tapping mode AFM was used for topographic analysis. The KPFM measurements were carried out using a 2 V AC signal at 20 kHz frequency applied to the sample by the inter lock-in amplifier in non-contact mode. The surface potential values were determined at the top of the measured fibers as this region has minimal height induced error.

### 2.7. Zeta Potential measurement

The zeta potential of the PCL samples was measured using an electrokinetic analyzer for solid surfaces (SurPASS, Anton Paar, Austria) with an adjustable gap cell [19]. Titration curves were obtained by zeta potential measurements in a 0.001 M KCl electrolyte solution. The pH variation from 3 to 9 was obtained with a progressive addition of 0.05 M HCl or 0.05 M NaOH to the solution for the acidic and basic regions respectively. It was controlled through an automatic titration unit. Simulated body fluid (SBF) was prepared according to Ref. [20] and added dropwise to ultrapure water in order to reach pH 7.4 and conductivity of 18 $mS \cdot m^{-1}$ for zeta potential measurements at physiological pH (without titration).

### 2.8. Cell culture

Human osteoblast-like cells (MG-63) (Sigma Aldrich, UK) were used for the cell culture study at 37 °C and humidity of 95% in 5% $CO_2$ atmosphere, with a density of $2 \times 10^4$ cells. Cells were cultured in modified eagle medium (MEM) supplemented with 10% fetal bovine serum (FBS), 1% amino acids, 1% glutamine, 2% penicillin-streptomycin (Sigma Aldrich, UK). Before cell seeding, samples were sterilized with UV light for 30 min.

### 2.9. SEM, 3D FIB – SEM tomography and energy-dispersive spectroscopy (EDX)

After 1, 3, and 7 days of incubation, cells were fixed with 2.5% glutaraldehyde solution in PBS (Sigma Aldrich, UK) and were incubated for 2 h. Prior to FIB-SEM tomography, cells were stained with a 1% $OsO_4$ solution in PBS (Sigma Aldrich, UK) for 30 min and rinsed in PBS afterward. The samples were dehydrated in 50%, 70%, 96%, and 100% ethanol solutions (analytical standard, Avantor, Poland) and finally with hexamethyldisilazane (HMDS) (Sigma Aldrich, UK) overnight. Then, they were coated with approximately 5 nm and 20 nm gold layer for the SEM and FIB-SEM tomography respectively, using a rotary-pumped sputter coating (Q150RS, Quorum Technologies, UK). SEM imaging was carried out at a voltage of 3 kV and a current of 30 pA. The 3D tomography of the cell interactions with the PCL fibers was achieved with FIB-SEM (NEON CrossBeam 40EsB, ZEISS, Germany), using the $Ga^+$ ion beam at a current of 20 pA and voltage of 30 kV. SEM images of the cross-sectioned samples were taken at a current of 500 pA and voltage of 3 kV. The 3D reconstructions were obtained using Avizo 8.1 software.

To verify early collagen mineralization EDX spectra were obtained using EDS detector Quantax 800 (Bruker, Germany), at a current of 200 pA and a voltage of 10 kV. Three points were analyzed for each sample, indicating collagen, cells' surface and fibers.

### 2.10. Tomographic microscopy

Tomographic microscopy (NanoLive 3D Cell Explorer Fluo, Switzerland) was used for the live imaging of cells. Fibers were electrospun onto 14 mm glass cover slides for 30 s to deposit only single fibers on the surface. Sterilized slides were placed into 35-mm Ibidi glass bottom μ-Dish dishes (Ibidi GmbH, Germany). Next, 5000 cells were seeded per dish and cultured for 24 h. Images were taken using STEVE FULL software (ver. 1.6.3496, Switzerland). The movies 1 and 2 from NanoLive are available in the Supplementary files.

### 2.11. Cell adhesion study

Initial cell adhesion was studied after 1, 2 and 4 h of incubation. The fixed cells were stained with 0.5 mL of 10 $\mu g \cdot mL^{-1}$ Hoechst solution (Thermo Fisher Scientific, USA) for 30 min and rinsed in PBS afterwards. Fluorescence imaging was achieved using an inverted light microscope IB-100 (Delta Optical, Poland) with a fluorescence lamp. Cells were counted from fluorescence microscope images using Fiji (Life-Line Version 2.0., USA). Cell capture efficiency was calculated using the following Eq. [21]:

$$\text{Cell capture efficiency} = \frac{N_0 S}{N S_0} \cdot 100\% \quad (1)$$

where $N$ is the number of cells seeded on the samples, $N_0$ is the average cell number counted from the image, $S$ is the surface area of the sample and $S_0$ is the image area.

### 2.12. Collagen staining and imaging

Collagen formation was investigated on cells after 1, 3, and 7 days in culture. The solution for collagen staining was prepared by dissolving 50 mg of Sirius Red 80 in 50 ml of saturated picric acid (Sigma Aldrich, UK). A 2 ml volume of Sirius Red solution was added onto the fixed sample. After 1 h of incubation the samples were rinsed with distilled water and air dried. Imaging was performed using a light microscope Axio Imager M1m (Zeiss, Germany). The staining solution was extracted with 1 ml of 0.1 M NaOH (Sigma Aldrich, UK) for 1 h in 25 °C, with shaking. Absorbance was measured with an automatic Microplate Reader LT-400 (Labtech, UK) with a 540 nm wavelength.

### 2.13. Alzarin Red S (ARS) staining

Calcium mineralization was investigated on the PCL samples after 7, 14, and 21 days of cell culture. The culture medium was removed from each sample and washed 3 times in PBS. Cells were fixed using a 4% formaldehyde solution (Sigma Aldrich, UK), incubated for 15 min and washed with deionized water afterward. Next, 250 μL of 40 mM ARS (ScienCell, CA) solution was added per well and incubated for 30 min. ARS dye was removed by rinsing 5 times in deionized water. The imaging of the dried samples was achieved using light microscope Axio

Imager M1m (Zeiss, Germany) at a magnification of 20× with extended focus (z-stack) mode, with 3 μm step.

### 2.14. Statistical analysis

The average fiber diameter and fiber porosity were calculated from 100 measurements taken from SEM images. The $R_a$ parameter was calculated as a mean of 10 independent analyses per sample, and the contact angles were measured on ten droplets for each liquid. The zeta potential was measured with four repetitions for each time and pH point. Capture percentage was calculated from 10 images from fluorescence microscopy and absorbance was given as an average value calculated from six repetitions per sample. The statistical analysis was performed in OriginPro (ver. 2020b, USA). The errors are based on the standard deviation. A one-way ANOVA, followed by Tukey's post-hoc test [2] was used for statistical analysis, and values were considered to be significantly different when $p < 0.05$.

## 3. Results and discussion

### 3.1. Surface properties of PCL fibers

Smooth and porous PCL fibers were electrospun with positive, PCL (+) and negative, PCL (−) voltage polarities. The smooth fibers showed similar morphology and an average fiber diameter of 3.9 ± 1.6 μm and 3.7 ± 1.1 μm for PCL (+) and PCL (−) respectively. Porous fibers were obtained due to the addition of DMSO to the polymer solution and increasing humidity up to 70% during electrospinning [22]. Fiber produced with positive voltage polarity are usually characterized by higher average fiber diameters [23]. The addition of DMSO lowered the evaporation rate while maintaining a high humidity in the chamber, and this was found to affect the diameter of obtained fibers. Therefore, the porous fibers showed fiber diameter of 1.9 ± 0.8 μm for PCL (+) and 2.5 ± 0.5 μm for PCL (−), see Fig. 1. The surface roughness of the PCL fibrous mats was analyzed by profilometry study using laser microscopy images (Supplementary Fig. S1) with average values of $R_a$ = 4.8 ± 0.4 μm and $R_a$ = 5 ± 0.8 μm for the smooth PCL (+) and the PCL (−) fibers, whereas $R_a$ = 1.2 ± 0.2 μm and $R_a$ = 1.8 ± 0.1 μm for the porous PCL (+) and PCL (−). The size of the pores on the porous PCL fiber surface was found to be in the range from 0.2 to 2 μm. The decreased $R_a$ of porous fibers was attributed both to the lower fiber diameter and surface porosity. [24,25]. The wetting properties of the PCL film and fibers indicated hydrophobic behavior, however, the contact angle decreased on the porous fibers, due to their lower $R_a$ [2,25]. This is similar to a report by Amrei et al. who found that the apparent contact angle decreases with fiber roughness [26]. The contact angle (⊖) results for three different probe liquids, namely water, PBS, and DMEM, measured on porous PCL(+) and PCL(−) fibers are presented in Supplementary Table S1.

### 3.2. The relation between surface and zeta potential and surface chemistry

KPFM was used to measure the surface potential of the PCL samples in air. The surface topography recorded with AFM (Fig. 2A–E) was measured simultaneously with the map of the surface potential (Fig. 2F–J). The surface potential was estimated to be 554.7 ± 12.8 mV and 574.4 ± 11.2 mV for the smooth PCL (+) and the PCL (−) fibers, whereas it was estimated to be 588.7 ± 10.2 mV and 685.9 ± 12.3 mV for the porous PCL (+) and PCL (−) fibers. The PCL film used as a reference sample showed a potential of 220.6 ± 6.7 mV which was significantly lower than the values obtained for PCL fibers. It is important to note that the PCL film was spin-coated without an external electric field being present, as opposed to an electric field being present during the fabrication of the electrospun PCL fibers.

The surface chemistry of the PCL fibers and the film was examined with ARXPS, showing an increased average O=C/O-C intensity ratio on the smooth PCL (−), due to the repulsion of electronegative double-bonded oxygen from the fiber surfaces (Table 1). The fitting parameters and the ARXPS details are presented in Supplementary Fig. S2. The higher O=C/O-C intensity ratio in porous fibers can be related to the surface roughness, as the XPS take-off angle was set to 15° to obtain information from the topmost layer of the material. These results confirmed that changing voltage polarity during electrospinning allows for polymer chain reorientation [15,18]. Additionally, it enables controlling the surface chemistry and the electric potential of the electrospun fibers, as the KPFM results were found to be correlated with the ARXPS data, showing higher surface potential for fibers produced with negative voltage polarity due to the decreased oxygen content on the fibers surface. Similarly, the two times higher surface potential of 145 mV was obtained for the PCL fibers produced with negative polarity in comparison to fibers produced with positive polarity, showing a potential of 74 mV [2]. A similar effect was observed for the PVDF fibers showing −95 mV and −173 mV, caused by increased fluorine content for the fibers electrospun applying positive voltage polarity [16]. The surface potential of the polarized PVDF coated titanium substrate (PTi) was measured with KPFM showing −930 ± 12 mV and a zeta potential of approximately −45 mV. The charged PTi surfaces induced cell adhesion, proliferation, and osteogenic differentiation [27].

Separately, the zeta potential of the PCL fibers and film were measured in contact with two diluted saline solutions: a standard KCl solution, to investigate zeta potential evolution vs pH in a solution where adsorption of ions from the solution is minimal [24], and a diluted SBF, to investigate surface behavior at fixed pH, in a simulated physiological condition [19]. From the titration curves (Fig. 2L) obtained by measuring zeta potential as a function of the pH in the KCl solution, the IEPs of the PCL samples were determined (Table 1). These measurements were considered reliable for the smooth fibers and the film, however, in the case of porous fibers the high water uptake capability was found to affect the obtained data. The IEP is close to 4 on a neutral surface without functional groups. The IEP is shifted towards lower values if the acidic groups are on the surface, or to higher values if basic groups are present [24].The IEPs of the film and the PCL (+) sample are very close (around 3.4) and this can be correlated with the presence of acidic functional groups, while there is a shift towards the IEP of a neutral surface (pH around 4) in the case of the PCL (−) fibers. The difference in the IEP can be correlated to the change in O=C/O-C intensity: esters act like a very weak Lewis acid (pKa ~ 25) when the amount of C=O groups is reduced, as in the case of the PCL (−) fibers. It means that some units have an ether group instead of the ester, and the ethers act like a weak Lewis base justifying a shift of IEP towards pH 4. In KCl, PCL(+) fibers and PCL film show a small plateau in the basic region, which can be associated with the presence of functional groups (esters) with an acidic behavior giving the ability of the groups to become negatively charged in a basic environment [24]. The presence of this plateau is in accordance with the previously discussed IEP. The plateau is almost absent for PCL (−) fibers, comparably with the shift of the IEP near to 4 and the reduction of acidic functional groups. This investigation is important, as the acidic or basic behavior of the surface functional groups significantly influences the biological response to the material upon contact with the physiological fluids [28]. Moreover, the slope of the zeta potential titration curve in the KCl is higher in the case of the PCL (−) smooth fibers according to a higher hydrophobicity of these surfaces and a lower amount of polar functional groups [24]. Comparing the surface charge at physiological pH (7.4) measured in the KCl solution, the PCL (−) fibers have a higher absolute value of zeta potential compared to the PCL (+), analogously to KPFM data. The increase of the zeta potential on the fibers produced with negative voltage polarity is related to the higher O=C/O-C intensity ratio (see Fig. 2N). The PCL film was used as a reference sample, showing the zeta potential of −64 ± 1 mV. Previous studies showed that in physiological conditions, electrospun PCL fibers have a negative zeta potential of −52.7 mV and IEP of 3.0 [29], whereas the PCL film measured in the $KNO_3$ solution

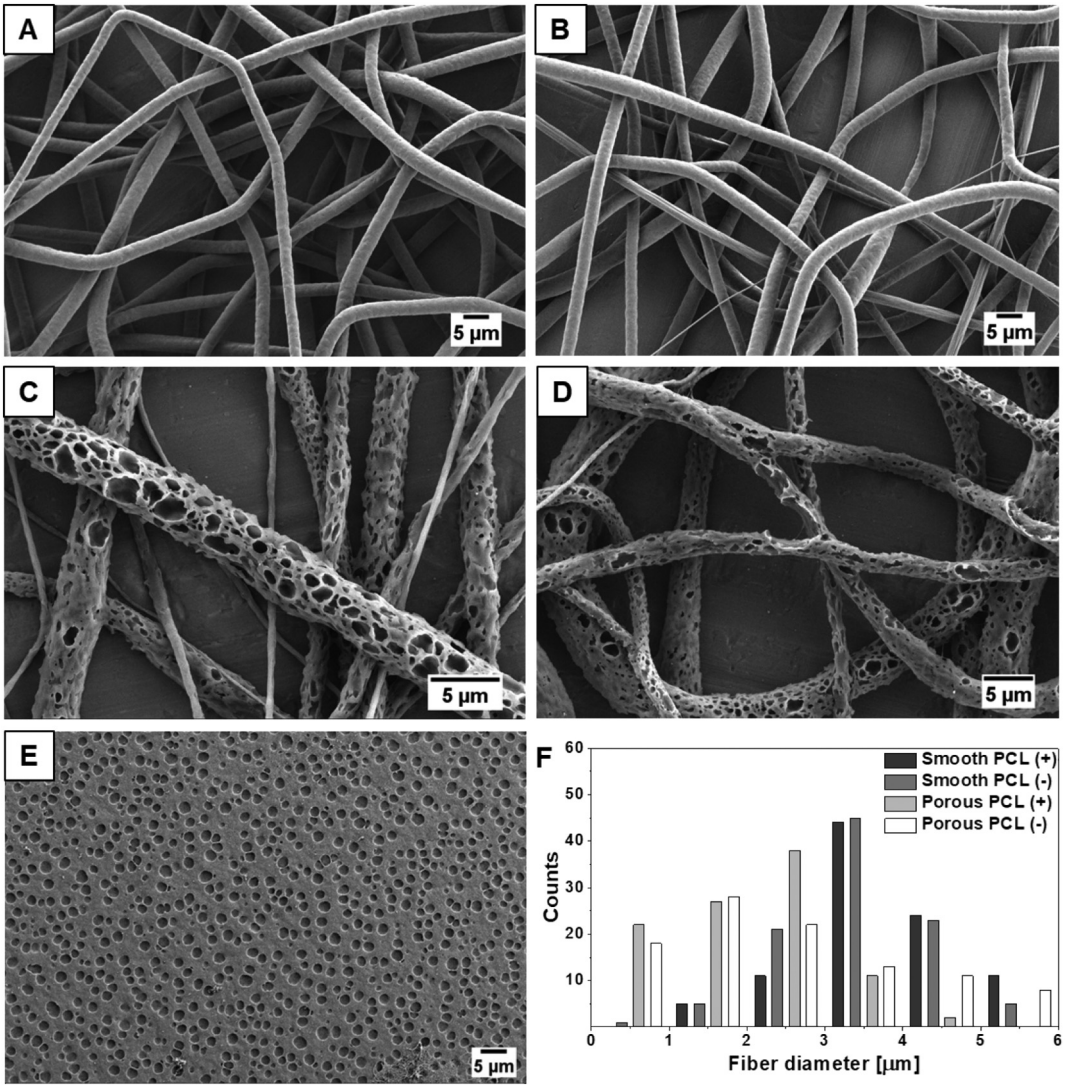


**Fig. 1.** SEM micrographs of A) and B) smooth, C) and D) porous PCL (+) and PCL (−) respectively, E) PCL film, and F) histogram of PCL fiber diameter distribution.

shown IEP of 4.0 [30]. The above cited difference among the smooth PCL (+) and PCL (−) fibers, in terms of IEP and the absolute value of the surface charge at the physiological pH (in KCl solution), have not been observed for the porous fibers. Since in the literature there is no evidence for surface roughness influence on surface charge [31], this behavior can be associated with the water uptake capability of these fibers (correlated with their high porosity). This phenomenon can affect the bulk material conductance and consequently the measured zeta potential. In the materials which expose acidic groups, the zeta potential curve is often shifted to less negative values [31]. The adsorption of the electrolyte in porous materials during zeta potential measurements and the consequent variation of the material conductance, which affect the zeta potential result, are widely discussed in the literature and should be taken into account in the interpretation of the results [32,33]. For this reason, zeta potential measurements on porous fibers give important information about their behavior in contact with fluids, but cannot be considered completely reliable from a quantitative standpoint, due to the experimental setup used.

When analyzing surface charge at the physiological pH, as measured in the diluted SBF, in the case of smooth PCL fibers, the behavior seems opposite to the one observed in KCl (the absolute value of the surface charge is higher for the PCL (+) than for the PCL (−)). In this case, the result can be considered reliable and attributed to the adsorption of ions (mainly $Ca^{2+}$ ions onto the negatively charged PCL surfaces) from the electrolyte (SBF), which is particularly pronounced on the fibers with a higher negative surface charge. Ion adsorption phenomena are normally negligible in KCl media, which are designed to avoid electrolyte-surface interactions [31]. In the SBF environment a rapid $Ca^{2+}$ adsorption at the beginning of the measurement can be supposed, without significant variation in time (Fig. 2M).In the case of porous fibers the values of the surface charge at the physiological pH, measured in the diluted SBF, are almost equal for both types of fibers. This behavior can be attributed to the effect of the electrolyte uptake discussed above.

With KPFM, we measured the direct electric potential of the fiber surface in air, confirming the molecular reorientation inside the fiber when a negative voltage polarity is applied during electrospinning. However, surface potential does not remain static under physiological conditions, thus it must be correlated with the zeta potential formed upon the materials' contact with a liquid environment. In this case, zeta potential measurements are found in correlation with the KPFM results showing higher absolute values of surface electrical and zeta potential for the fibers produced with negative voltage polarity, when measured in an electrolyte solution which does not interact with the fibers surface. In SBF environment a rapid $Ca^{2+}$ adsorption at the beginning of the measurement can be assumed, without significant

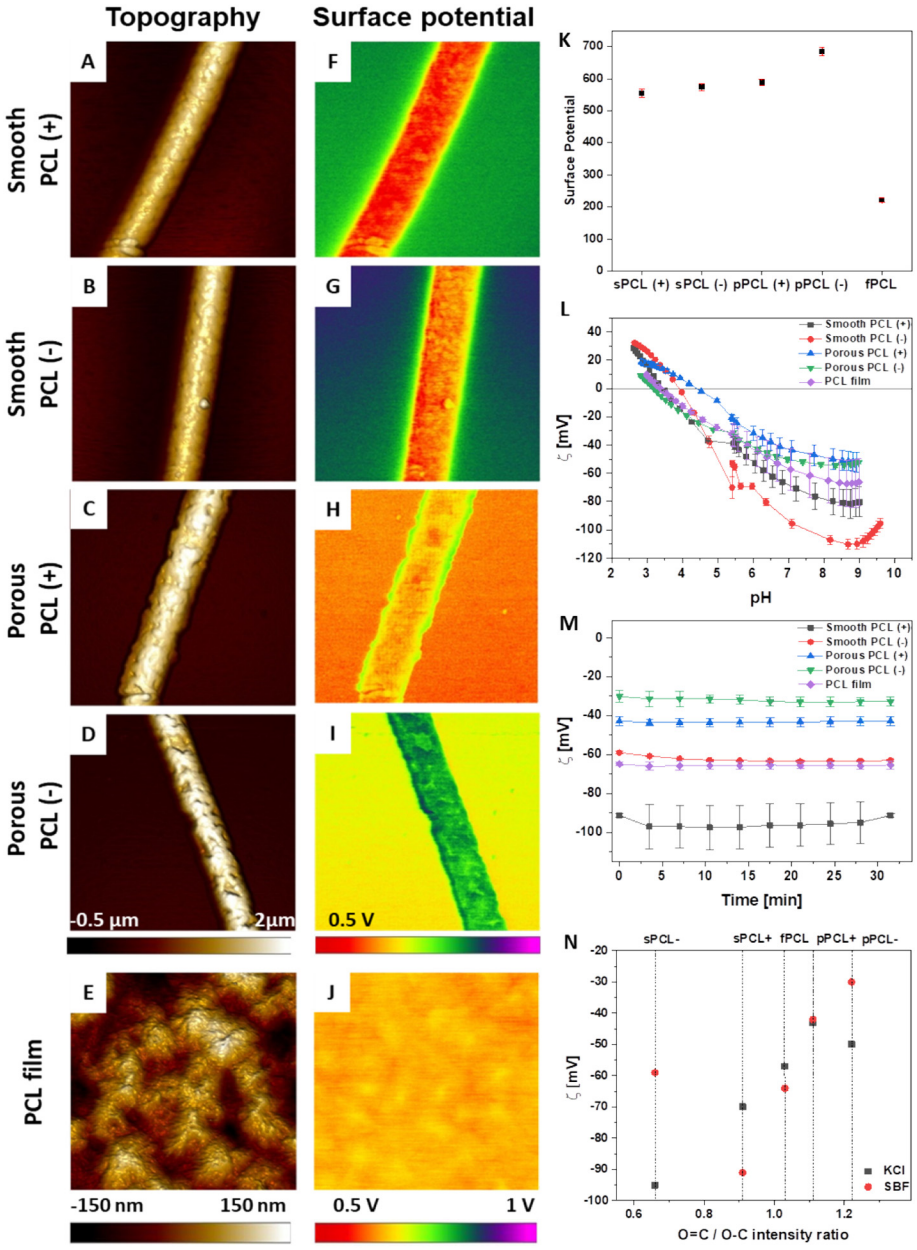


**Fig. 2.** KPFM results showing A–E) surface topography, F–J) map of the surface potential for the smooth PCL (+) and PCL (−)the porous PCL (+) and the PCL (−) fibers and the PCL film, K) the graph of the surface potential measured with the KPFM L) titration curves measured in the function of pH in KCL solution M) ζ in the function of time in the SBF solution in pH 7.4, and N) ARXPS surface chemistry showing close to the linear relation of the O=C/O-C intensity ratio and the measured zeta potential.

**Table 1**
A summary of the isoelectric point (IEP) and the XPS results showing the surface chemistry averaged O=C/O-C intensity ratio.

| Sample | IEP | XPS -surface chemistry averaged O=C/O-C intensity ratio |
|---|---|---|
| Smooth PCL (+) | 3.45 | 0.91 |
| Smooth PCL (−) | 3.91 | 0.66 |
| Porous PCL (+) | 4.41 | 1.11 |
| Porous PCL (−) | 3.18 | 1.22 |
| PCL film | 3.38 | 1.03 |

variation in time (Fig. 2M). On the other hand, an evolution of surface charge due to $Ca^{2+}$ adsorption from diluted SBF during the measurements was previously observed by the authors for bioactive materials [19].

### 3.3. Cell – material interaction

Cell morphology was investigated with SEM, following cell culture on the surface of smooth, porous PCL fibers and on PCL film for 1, 3, and 7 days (see Fig. 3). From the first day itself, cells were found to proliferate on the smooth fibers, attaching to the scaffold surface via filopodia. These were significantly longer in the case of cells growing

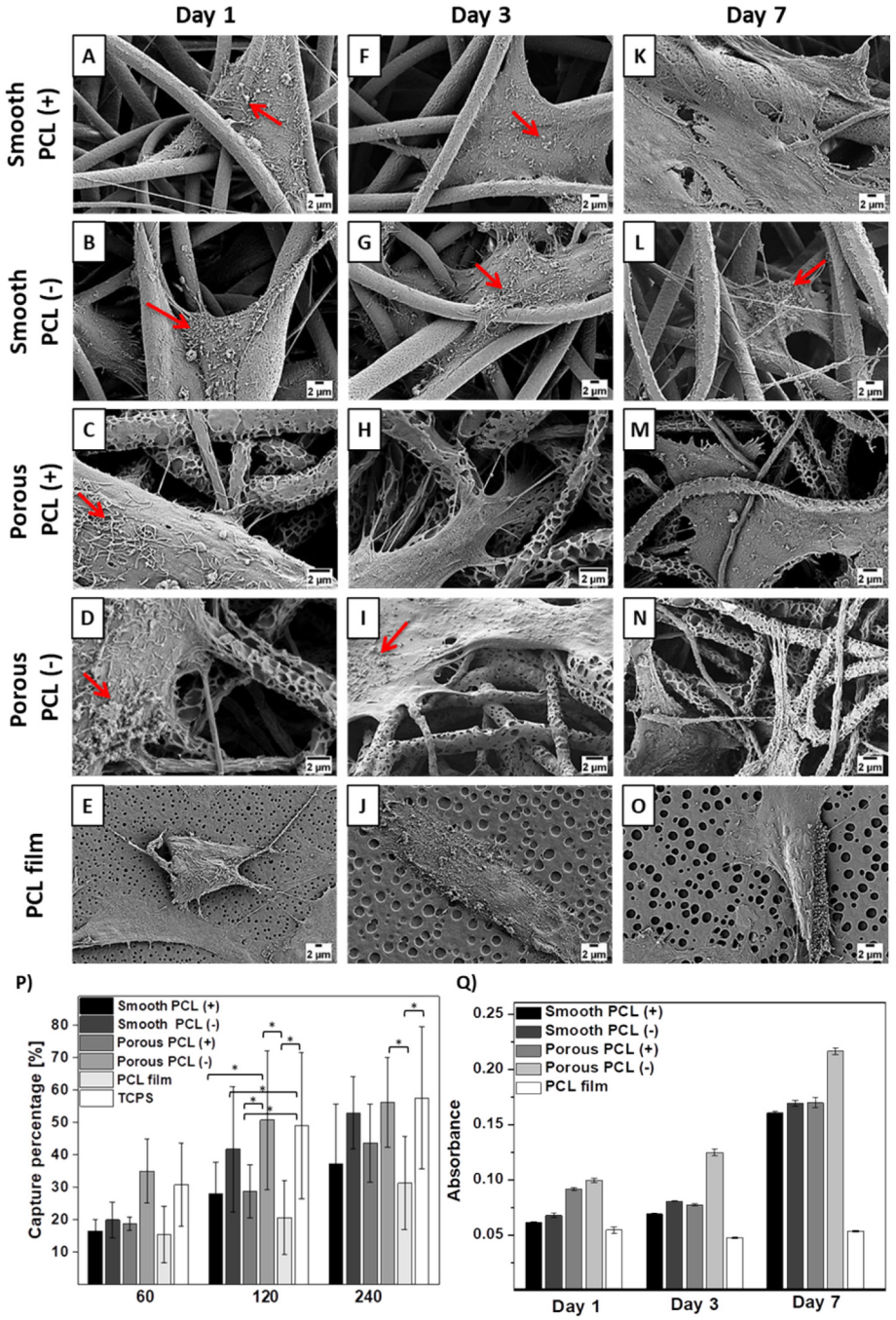


**Fig. 3.** SEM micrographs of cells growing on smooth, porous PCL fibers and after: A–E) 1, F–J) 3 and K—O) 7 days of culture (red arrows indicate collagen fibrils), P) Graph of the capture percentage of the cells adhered after 1, 2, and 4 h and Q) Sirius Red absorbance indicating collagen formation after 1, 3 and 7 days of cell culture on the smooth PCL (+), PCL (−), the porous PCL (+) and the PCL (−) and the PCL film. Statistical significance was calculated with a one-way ANOVA followed by a post – hoc Tukey test with a significance level $p < 0.05$. In Panel Q the significant difference presented among all the tested groups. (For interpretation of the references to color in this figure legend, the reader is referred to the web version of this article.)

on the scaffolds with a higher potential, PCL (−) (see Fig. 3B, D). With increasing culture time, we observed cell migration inside the scaffolds (Fig. 3F–G, K–L). In the case of the PCL fibers with higher surface potential, cell filopodia were often found to be overlapping the fiber surface, thus increasing their attachment points. Additionally, the cells growing on the porous scaffolds formed a greater number of filopodia preferring rough surfaces (see Fig. 3C–D) for their attachment [34,35]. The cells on the smooth and porous PCL (−) scaffolds were found to be more likely to migrate inside the scaffolds (Fig. 3L–N). On the porous PCL fibers, the cells formed not only extended filopodia to attach the surface, but also many supporting lamellipodia to adhere to the pores. However, on the PCL films, cells were mostly spheroid, showing poor filopodia formation, thus suggesting weak adhesion to the flat surface, as shown in Fig. 3E.

With 3D FIB-SEM tomography we showed in great detail the cell-material integration at a submicron level, surpassing the resolution of other microscopy and tomography techniques [36]. The 3D visualization of cell integration with individual fibers produced with negative voltage polarities during electrospinning indicated that on smooth fibers, cells adapted the space between the fibers, forming long filopodia to attach and overlap the fiber surface (Fig. 4A). Cells on the porous PCL (−) fibers internalized the open pores on the surface, forming supporting lamellipodia integrating with the pores, thus suggesting

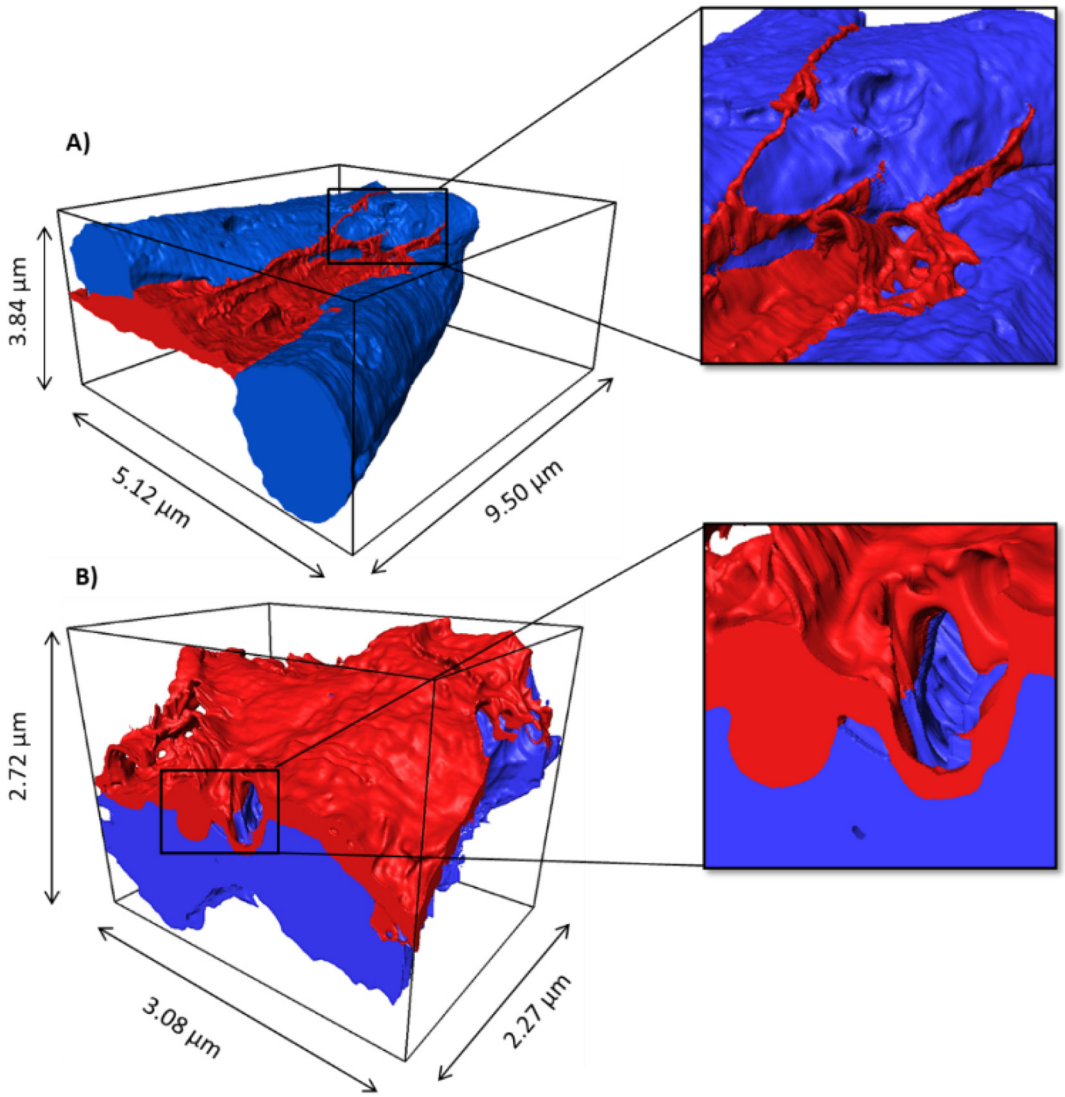


**Fig. 4.** 3D reconstructions from FIB-SEM tomography of cell interaction with the scaffolds after 3 days of culture: A) cell attached to the smooth PCL (—) scaffold, growing between the fibers with zoom in on long filopodia overlapping the fibers and B) cell growing on top of the fibers with zoom in on cell internalizing the pores on the surface of the porous PCL (—) scaffold. The voxel size of the 3D reconstructions was 10 × 10 × 30 nm and 5 × 5 × 15 nm for the smooth and the porous PCL (—) scaffolds, respectively. Cells in red and fibers in blue. See the animation with the reconstructions in the Movie 3 and 4 in the Supplementary files. (For interpretation of the references to color in this figure legend, the reader is referred to the web version of this article.)

better cell adhesion in this 3D environment (Fig. 4B). Similar behavior was confirmed with the live imaging of the cells (see Supplementary Fig. S3). On the smooth PCL (—), cells grew along the fibers forming elongated filopodia to attach the surface, whereas on the porous PCL (—) we observed a greater number of formed filopodia and lamellipodia internalizing the pores on the fiber surfaces.

The initial cell adhesion was examined measuring the cell capture efficiency at early time points. After 1 h, the greatest cell number adhered to the surface of the porous PCL (—) fibers whereas for other fibers the results were lower. Additionally, the number of cells that were adhered to the porous PCL (—) fibers was similar to that observed on the surface of tissue culture polystyrene (TCPS). Increasing the cell incubation time resulted in increased cell adhesion and after 2 h the highest cell number was again found on the porous PCL (—) fibers and TCPS, with a capture efficiency of approximately 50%. After 4 h we noticed a similar cell adhesion on both the smooth and the porous PCL (—) fibers and the TCPS (see Fig. 3P). The lowest cell adhesion was indicated on the flat PCL film surfaces at all of the tested time points, confirming that the 3D structure of the electrospun fiber scaffolds favors osteoblast-like cell adhesion. The fluorescence microscopy images used for the adhesion measurements are presented in Supplementary Fig. S4. The high standard deviation in Fig. 3P, can be explained with the limited time for cells to uniformly spread throughout the samples.

Initial cell adhesion plays a critical role in cell communication, tissue development, and is determined by electrostatic forces [37]. Our results demonstrate that initial cell adhesion was determined both by surface charge and surface topography, as more cells adhered to the fibers with higher surface potential and a higher capture percentage of cells was observed on the porous scaffolds (see Fig. 3P). In the study of Xu et al. NIH-3T3 fibroblasts were incubated from 15 to 120 min on the positively and negatively charged silica biointerfaces with the same topography [38]. The results showed higher initial cell adhesion on the positive surfaces, due to the electrostatic attraction between the negatively charged cells and the positive surface. In our study, greater cell adhesion was observed on scaffolds with higher absolute value of surface potential, as all the PCL surfaces were negatively charged [38]. This was also confirmed with other studies for rat marrow stromal cells [39]. Higher pre-osteoblastic cell adhesion was reported on porous

electroactive micropatterned PVDF scaffolds, promoting their growth and regeneration of bone tissue [40]. Other groups examined the PVDF –(trifluoroethylene) (PVDF-TrFE) membranes modified with $BaTiO_3$ nanoparticles, that were poled to reach the natural endogenous biopotential of −76.9 mV. The result showed that maintaining the electric bioenvironment encouraged the osteogenic behavior of the BM-MSCs in vitro and enhanced bone defect healing in vivo [41].

A key factor in bone regeneration is the collagen mineralization process, crucial for further apatite formation [42] and osteointegration [34]. To study the influence of surface potential on the collagen formation, we increased the culture time up to 7 days. The formation of collagen fibrils on the cell surfaces was indicated already after the first day of culture, as analyzed with SEM (see Fig. 3). Collagen was present on the surface of the smooth and porous PCL fibers and the film. We confirmed the collagen formation with Sirius Red staining, showing higher absorbance on the porous compared to the smooth PCL fibers already on the first day of culture (see Fig. 3Q). As expected, with increasing culture time, more collagen was formed on the cell surfaces, as was observed in the light microscopy images (Fig. 5). Higher collagen formation was noticed for the porous fibers after the first and third day of culture. The lower absorbance value for the porous PCL (+) on the third day was due to sample folding what was limiting the rinsing step of the stained sample in the standard protocol. On day 7, the collagen formation increased and significantly higher absorbance was observed on the porous PCL (−) comparing to other samples. The low absorbance observed for the PCL film in comparison confirmed the great impact of the 3D architecture of the electrospun fibers, as well as their surface charge and fiber porosity on collagen formation. Statistical significance occurred in all of the tested groups (Fig. 3Q), however, it was not indicated on the graph, as it made it illegible. Light microscopy images showed higher intensity of red, indicating collagen, for the fibers with higher surface potential (PCL (-)). Additionally, enhanced red coloring on cells was noticed for the porous PCL fibers.

### 3.4. Calcium mineralization

Biomineralization is a natural, biological process of apatite formation that can be mimicked in vitro, involving the controlled calcium phosphates nucleation from the solution [43]. After 7 days of culture, the mineral accumulation was formed on the cell surfaces (see Supplementary Fig. S5). The EDX analysis confirmed the Ca and the P presence in the mineral depositions, suggesting collagen mineralization [44]. The

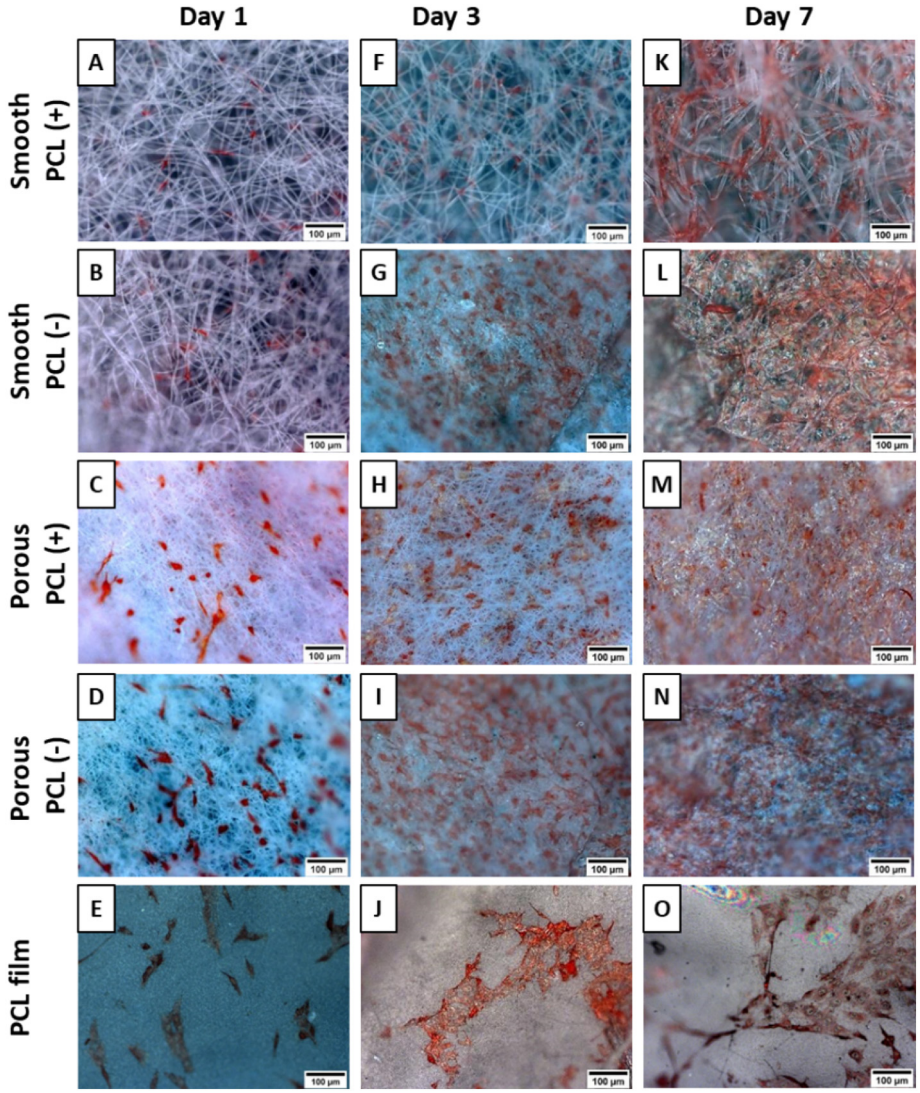


**Fig. 5.** Light microscopy images of the collagen stained with Sirius Red assay (indicated in red) A–E) after 1 day, F–J) 3 days, and K–O) 7 days of cell culture on the surface of the smooth PCL (+), the smooth PCL (−), the porous PCL (+), and the porous PCL (−) fibers and PCL film. (For interpretation of the references to color in this figure legend, the reader is referred to the web version of this article.)

Au in the EDX spectra arises due to the coating on the samples, while the appearance of Si is an artefact. In our study we also used ARS staining to evaluate calcium-rich deposits by cells in culture after 7, 14, and 21 days. The light microscopy images of the PCL samples after ARS staining are shown in Supplementary Fig. S6. The red color corresponds to the presence of calcium and was observed on the PCL scaffolds already after 7 days of cell culture. With increasing culture time higher intensity of red was noticed, suggesting greater calcium mineralization. The quantitative measurement of calcium mineralization on PCL scaffolds was not provided due to the difficulties in ARS extraction from the 3D fibrous constructs. The stained PCL samples after 7, 14 and 21 days are presented in Supplementary Fig. S7. Calcium mineralization was observed both on the smooth, the porous PCL fibers, and the film. Comparatively higher mineralization was noticed on the porous than on the smooth PCL scaffolds, as surface porosity encourages the mineral nucleation [45]. The rapid and high calcium mineralization throughout the cell culture time was promoted by the negative zeta potential of the PCL samples in the physiological conditions (see Fig. 2 M). Biominerals form calcium ions within proteinaceous matrices containing negatively charged functional groups, attracting the positive, $Ca^{2+}$. This interaction immobilizes the ions, causing nucleation of the minerals [46]. As the $Ca^{2+}$ ions accumulate the surface becomes positive and combines with the negatively charged phosphate ions, forming metastable, amorphous calcium phosphate, that next transforms into stable, crystalline apatite [47]. The higher the negative surface charge, and hence zeta potential, the greater mineralization in vitro [47]. The electrostatic accumulation of $Ca^{2+}$ ions near the negative surface promotes HAp nucleation in the SBF and in the cell culture media, which is crucial for further tissue formation and bone regeneration [43,48].

## 4. Conclusions

In our study, we successfully produced scaffolds with different morphologies constructed from smooth and porous PCL fibers using a single-step approach of electrospinning. A novel approach of changing voltage polarity during electrospinning allowed control of surface charge, zeta potential and the surface chemistry of the PCL fibers. We showed that the surface potential of the PCL fibers together with the surface topography determine the initial cell adhesion, as a greater cell number was observed on the porous fibers with the higher surface potential. The higher surface potential enhanced the collagen mineralization that was observed after 7 days of culture. The negative zeta potential of the PCL samples in the physiological conditions (pH 7.4), promoted calcium mineralization, indispensable for HAp nucleation and further tissue formation in the regeneration process. This study has a great impact on the development of charged scaffolds for enhanced bone mineralization in tissue engineering. Our results show that determination of surface roughness and potential are key in controlling cell function and behavior in physiological conditions, and must be considered in designing biomaterials for specific applications.

## Data availability

The data supporting this article are found within the text and the supplementary information file. Any additional data and the data that support the plots within this paper are available from the corresponding author upon reasonable request.

## CRediT authorship contribution statement

**Sara Metwally:**Investigation, Formal analysis, Writing - original draft.**Sara Ferraris:**Formal analysis.**Silvia Spriano:**Formal analysis. **Mateusz M. Marzec:**Formal analysis.**Sung-Kyun Kim:**Formal analysis. **Andrzej Bernasik:**Formal analysis.**Sohini Kar-Narayan:**Formal analysis.**Urszula Stachewicz:**Methodology, Formal analysis, Writing - original draft.

## Declaration of competing interest

The authors declare that they have no known competing financial interests or personal relationships that could have appeared to influence the work reported in this paper.

## Acknowledgment

The studies were conducted within the 'Nanofiber-based sponges for atopic skin treatment' project, which is carried out within the First TEAM programme of the Foundation for Polish Science co-financed by the European Union under the European Regional Development Fund, project No POIR.04.04.00-00- 4571/18-00. The zeta potential study was conducted within the KMM-VIN Research Fellowship, call 2018. The microscopy study was supported by the infrastructure at International Centre of Electron Microscopy for Materials Science (IC-EM) at AGH University of Science and Technology. We thank Nanolive SA company for possibility to test Nanolive tomographic microscope on our samples. Piotr Szewczyk thanks Sonata Bis 5 project, No 2015/18/E/ST5/00230 for PhD scholarship. Magdalena Wytrwal - Sarna thanks Sonata 11 project, No 2016/21/D/ST5/01636. Sohini Kar-Narayan acknowledges support from the European Research Council through an ERC Starting Grant (Grant no. ERC–2014–STG–639526, NANOGEN).

## Appendix A. Supplementary data

Supplementary data to this article can be found online at https://doi.org/10.1016/j.matdes.2020.108915.

## References

[1] B. Finke, F. Luethen, K. Schroeder, P.D. Mueller, C. Bergemann, M. Frant, A. Ohl, B.J. Nebe, The effect of positively charged plasma polymerization on initial osteoblastic focal adhesion on titanium surfaces, Biomaterials 28 (2007) 4521–4534, https://doi.org/10.1016/j.biomaterials.2007.06.028.
[2] S. Metwally, J.E. Karbowniczek, P.K. Szewczyk, M.M. Marzec, A. Gruszczyński, A. Bernasik, U. Stachewicz, Single-step approach to tailor surface chemistry and potential on electrospun PCL fibers for tissue engineering application, Adv. Mater. Interfaces 6 (2018) 1801211, https://doi.org/10.1002/admi.201801211.
[3] E. Mariani, G. Lisignoli, R.M. Borzì, L. Pulsatelli, Biomaterials: foreign bodies or tuners for the immune response? Int. J. Mol. Sci. 20 (2019) 636, https://doi.org/10.3390/ijms20030636.
[4] D. Cho, S. Lee, M.W. Frey, Characterizing zeta potential of functional nanofibers in a microfluidic device, J. Colloid Interface Sci. 372 (2012) 252–260, https://doi.org/10.1016/j.jcis.2012.01.007.
[5] P. Novák, V. Havlíček, Protein extraction and precipitation, in: P. Ciborowski, J. Silbering (Eds.), Proteomic Profiling Anal. Chem. Crossroads, 2nd ed.Elsevier B.V 2016, pp. 51–62, https://doi.org/10.1016/B978-0-444-63688-1.00004-5.
[6] K. Cai, M. Frant, J. Bossert, G. Hildebrand, K. Liefeith, K.D. Jandt, Surface functionalized titanium thin films: zeta-potential, protein adsorption and cell proliferation, Colloids Surfaces B Biointerfaces 50 (2006) 1–8, https://doi.org/10.1016/j.colsurfb.2006.03.016.
[7] D.R. Schmidt, H. Waldeck, W.J. Kao, Protein adsorption to biomaterials, in: D.A. Puleo, R. Bizios (Eds.), Biol. Interact. Mater. Surfaces, Springer, New York 2009, pp. 1–18, https://doi.org/10.1007/978-0-387-98161-1_1.
[8] J. Skvarla, A physico-chemical model of microbial adhesion, J. Chem. Soc. 89 (1993) 2913–2921, https://doi.org/10.1039/ft9938902913.
[9] L. Marcotte, M. Tabrizian, Sensing surfaces: challenges in studying the cell adhesion process and the cell adhesion forces on biomaterials, IRBM 29 (2008) 77–88, https://doi.org/10.1016/j.rbmret.2007.11.019.
[10] S. Boonrungsiman, E. Gentleman, R. Carzaniga, N.D. Evans, D.W. Mccomb, A.E. Porter, M.M. Stevens, D.W. Mccomba, S. Boonrungsiman, E. Gentleman, E. Porter, M.M. Stevensa, The role of intracellular calcium phosphate in osteoblast-mediated bone apatite formation, Proc. Natl. Acad. Sci. U. S. A. 109 (2012) 14170–14175, https://doi.org/10.1073/pnas.1208916.
[11] F. Nudelman, A.J. Lausch, N.A.J.M. Sommerdijk, E.D. Sone, In vitro models of collagen biomineralization, J. Struct. Biol. 183 (2013) 258–269, https://doi.org/10.1016/j.jsb.2013.04.003.
[12] F. Tan, J. Liu, K. Song, M. Liu, J. Wang, Effect of surface charge on osteoblastic proliferation and differentiation on a poly(ethylene glycol)-diacrylate hydrogel, J. Mater. Sci. 53 (2018) 908–920, https://doi.org/10.1007/s10853-017-1558-8.
[13] S.A. Theron, E. Zussman, A.L. Yarin, Experimental investigation of the governing parameters in the electrospinning of polymer solutions, Polymer 45 (2004) 2017–2030, https://doi.org/10.1016/j.polymer.2004.01.024.
[14] M.M. Hohman, M. Shin, G. Rutledge, M.P. Brenner, G. Rutledge, Electrospinning and electrically forced jets. I. Stability theory electrospinning and electrically forced jets. I. Stability theory, Phys. Fluids 13 (2001)https://doi.org/10.1063/1.1383791.

[15] U. Stachewicz, C.A. Stone, R. Willis, A.H. Barber, C.R. Willis, A.H. Barber, Charge assisted tailoring of chemical functionality at electrospun nanofiber surfaces, J. Mater. Chem. 22 (2012) 22935–22941, https://doi.org/10.1039/C2jm33807f.
[16] P.K. Szewczyk, S. Metwally, J.E. Karbowniczek, M.M. Marzec, E. Stodolak-Zych, A. Gruszczynski, A. Bernasik, U. Stachewicz, Surface potential controlled cells proliferation and collagen mineralization on electrospun polyvinylidene fluoride (PVDF) fibers scaffolds for bone regeneration, ACS Biomater. Sci. Eng. 5 (2019) 582–593, https://doi.org/10.1021/acsbiomaterials.8b01108.
[17] H. Yoshimoto, Y.M. Shin, H. Terai, J.P. Vacanti, A biodegradable nanofiber scaffold by electrospinning and its potential for bone tissue engineering, Biomaterials 24 (2003) 2077–2082, https://doi.org/10.1016/S0142-9612(02)00635-X.
[18] T. Busolo, D.P. Ura, S.K. Kim, M.M. Marzec, A. Bernasik, U. Stachewicz, S. Kar-Narayan, Surface potential tailoring of PMMA fibers by electrospinning for enhanced triboelectric performance, Nano Energy 57 (2019) 500–506, https://doi.org/10.1016/j.nanoen.2018.12.037.
[19] S. Ferraris, S. Yamaguchi, N. Barbani, M. Cazzola, C. Cristallini, M. Miola, E. Vernè, S. Spriano, Bioactive materials: in vitro investigation of different mechanisms of hydroxyapatite precipitation, Acta Biomater. 102 (2020) 468–480, https://doi.org/10.1016/j.actbio.2019.11.024.
[20] T. Kokubo, H. Takadama, How useful is SBF in predicting in vivo bone bioactivity? Biomaterials 27 (2006) 2907–2915, https://doi.org/10.1016/j.biomaterials.2006.01.017.
[21] W. Liu, J. Zhan, Y. Su, T. Wu, C. Wu, S. Ramakrishna, X. Mo, S.S. Al-Deyab, M. El-Newehy, Effects of plasma treatment to nanofibers on initial cell adhesion and cell morphology, Colloids Surfaces B Biointerfaces 113 (2014) 101–106, https://doi.org/10.1016/j.colsurfb.2013.08.031.
[22] K.A.G. Katsogiannis, G.T. Vladisavljević, S. Georgiadou, Porous electrospun polycaprolactone (PCL) fibres by phase separation, Eur. Polym. J. 69 (2015) 284–295, https://doi.org/10.1016/j.eurpolymj.2015.01.028.
[23] H.W. Tong, M. Wang, Electrospinning of fibrous polymer scaffolds using positive voltage or negative voltage: a comparative study, Biomed. Mater. 5 (2010), 054110. https://doi.org/10.1088/1748-6041/5/5/054110.
[24] H.H. Kim, M.J. Kim, S.J. Ryu, C.S. Ki, young H. Park, Effect of fiber diameter on surface morphology, mechanical property, and cell behavior of electrospun poly(ε-caprolactone) mat, Fibers Polym 17 (2016) 1022–1042, https://doi.org/10.1007/s12221-016-6350-x.
[25] P.K. Szewczyk, D.P. Ura, S. Metwally, J. Knapczyk-Korczak, M. Gajek, M.M. Marzec, A. Bernasik, U. Stachewicz, Roughness and fiber fraction dominated wetting of electrospun fiber-based porous meshes, Polymers 11 (2019) 34, https://doi.org/10.3390/polym11010034.
[26] M.M. Amrei, M. Davoudi, G.G. Chase, H.V. Tafreshi, Effects of roughness on droplet apparent contact angles on a fiber, Sep. Purif. Technol. 180 (2017) 107–113, https://doi.org/10.1016/j.seppur.2017.02.049.
[27] Z. Zhou, W. Li, T. He, L. Qian, G. Tan, C. Ning, Polarization of an electroactive functional film on titanium for inducing osteogenic differentiation, Sci. Rep. 6 (2016) 35512, https://doi.org/10.1038/srep35512.
[28] S. Ferraris, M. Cazzola, V. Peretti, B. Stella, S. Spriano, Zeta potential measurements on solid surfaces for in vitro biomaterials testing: surface charge, reactivity upon contact with fluids and protein absorption, Front. Bioeng. Biotechnol. 6 (2018) 60–67, https://doi.org/10.3389/fbioe.2018.00060.
[29] O. Castan, J. Park, G. Jin, T. Kim, J. Kim, H. Kim, Angiogenesis in bone regeneration: tailored calcium release in hybrid fibrous scaffolds, ACS Appl. Mater. Interfaces 6 (2014) 7512–7522, https://doi.org/10.1021/am500885v.
[30] K. Wojciechowski, E. Klodzinska, Colloids and surfaces a: physicochemical and engineering aspects zeta potential study of biodegradable antimicrobial polymers, Colloids Surfaces A Physicochem. Eng. Asp. 483 (2015) 204–208, https://doi.org/10.1016/j.colsurfa.2015.04.033.
[31] T. Luxbacher, Dependences of the zeta potential, ZETA Guid. Princ. Streaming Potential Tech, 1st edAnton Paar GmbH, Graz, Austria 2014, pp. 46–71.
[32] P. Fievet, A. Szymczyk, C. Labbez, B. Aoubiza, C. Simon, A. Foissy, J. Pagetti, Determining the zeta Potential of porous membranes using electrolyte conductivity inside pores, J. Colloid Interface Sci. 235 (2001) 383–390, https://doi.org/10.1006/jcis.2000.7331.
[33] S. Potential, M. For, P. Media, A comparison of streaming and microelectrophoresis methods for obtaining the zeta Potential of granular porous media surfaces, J. Colloid Interface Sci. 209 (1999) 264–267, https://doi.org/10.1006/jcis.1998.5908.
[34] V. Karageorgiou, D. Kaplan, Porosity of 3D biomaterial scaffolds and osteogenesis, Biomaterials 26 (2005) 5474–5491, https://doi.org/10.1016/j.biomaterials.2005.02.002.
[35] H. Yuan, K. Kurashina, J.D. De Bruijn, Y. Li, K. De Groot, X. Zhang, A preliminary study on osteoinduction of two kinds of calcium phosphate ceramics, Biomaterials 20 (1999) 1799–1806, https://doi.org/10.1016/S0142-9612(99)00075-7.
[36] U. Stachewicz, T. Qiao, S.C.F. Rawlinson, F.V. Almeida, W.Q. Li, M. Cattell, A.H. Barber, 3D imaging of cell interactions with electrospun PLGA nanofiber membranes for bone regeneration, Acta Biomater. 27 (2015) 88–100, https://doi.org/10.1016/j.actbio.2015.09.003.
[37] S. Metwally, U. Stachewicz, Surface potential and charges impact on cell responses on biomaterials interfaces for medical applications, Mater. Sci. Eng. C. 104 (2019), 109883. https://doi.org/10.1016/j.msec.2019.109883.
[38] L.P. Xu, J. Meng, S. Zhang, X. Ma, S. Wang, The amplified effect of surface charge on cell adhesion by nanostructures, Nanoscale 8 (2016) 12540–12543, https://doi.org/10.1039/C6NR00649C.
[39] Q. Qiu, M. Sayer, M. Kawaja, X. Shen, J.E. Davies, Attachment, morphology, and protein expression of rat marrow stromal cells cultured on charged substrate surfaces, J. Biomed. Mater. Res. 42 (1998) 117–127, https://doi.org/10.1002/(SICI)1097-4636(199810)42:1<117::AID-JBM15>3.0.CO;2-I.
[40] T. Marques-Almeida, V.F. Cardoso, S. Ribeiro, F.M. Gama, C. Ribeiro, S. Lanceros-Méndez, Tuning myoblast and pre-osteoblast cell adhesion site, orientation and elongation through electroactive micropatterned scaffolds, ASC Appl. Biomater. 2 (2019) 1591–1602, https://doi.org/10.1021/acsabm.9b00020.
[41] X. Zhang, C. Zhang, Y. Lin, P. Hu, Y. Shen, K. Wang, S. Meng, Y. Chai, X. Dai, X. Liu, Y. Liu, X. Mo, C. Cao, S. Li, X. Deng, L. Chen, Nanocomposite membranes enhance bone regeneration through restoring physiological electric microenvironment, ACS Nano 10 (2016) 7279–7286, https://doi.org/10.1021/acsnano.6b02247.
[42] F. Nudelman, K. Pieterse, A. George, P.H.H. Bomans, H. Friedrich, L.J. Brylka, P.A.J. Hilbers, G. De With, N.A.J.M. Sommerdijk, The role of collagen in bone apatite formation in the presence of hydroxyapatite nucleation inhibitors, Nat. Mater. 9 (2010) 1004–1009, https://doi.org/10.1038/NMAT2875.
[43] V.S. Carvalho, E. Araujo, C.X. Resende, Effect of surface charge on the apatite mineralization process, Key Eng. Mater. 493–494 (2012) 513–518, https://doi.org/10.4028/www.scientific.net/KEM.493-494.513.
[44] G. Tomoaia, R. Pasca, On the collagen mineralization. A review, Clujul Med 88 (2015) 15–22, https://doi.org/10.15386/cjmed-359.
[45] P. Asanithi, Surface porosity and roughness of micrographite film for nucleation of hydroxyapatite, J. Biomed. Mater. Res. Part A. 102 (2014) 2590–2599, https://doi.org/10.1002/jbm.a.34930.
[46] K. Shuturminska, C.O. Malley, D.W.P. Collis, J. Conde, H.S. Azevedo, Displaying biofunctionality on materials through templated self-assembly, in: H.S. Azevedo, R.M.P. da Silva (Eds.), Self-Assembling Biomater. Mol. Des. Charact. Appl. Biol. Med, 1st ed.Elsevier Ltd 2018, pp. 341–370, https://doi.org/10.1016/B978-0-08-102015-9.00018-6.
[47] T. Kokubo, S. Yamaguchi, Chemical surface modification of a titanium scaffold, in: C. Wen (Ed.), Met. Foam Bone Process. Modif. Charact. Prop, 1st ed.Elsevier Ltd 2017, pp. 161–179, https://doi.org/10.1016/B978-0-08-101289-5.00006-8.
[48] P. Zhu, Y. Masuda, K. Koumoto, The effect of surface charge on hydroxyapatite nucleation, Biomaterials 25 (2004) 3915–3921, https://doi.org/10.1016/j.biomaterials.2003.10.022.